Computer simulation of the role of groundwater seepage in forming Martian valley networks

Wei Luo[1] and Alan D. Howard[2]

Received 7 August 2007; revised 29 January 2008; accepted 20 February 2008; published 10 May 2008.

[1] The role of groundwater in forming Martian valley networks is simulated in a computer model as seepage erosion by contributing to surface runoff and as seepage weathering by causing accelerated weathering of bedrock, which makes its subsequent erosion and removal easier. Simulation results show that seepage erosion cannot mobilize large grain size sediment and is marginally effective at generating integrated valley networks with realistic rates of aquifer recharge. On the other hand, seepage weathering may play a major role in forming Martian valley networks. Seepage weathering combined with fluvial runoff creates stubby deep canyons with abrupt headwalls that are similar in morphology to terrestrial and Martian valley systems attributed to erosion by groundwater. Depending on the relative contribution of groundwater weathering to surface runoff erosion, a continuum of valley network morphology can be generated. Eolian modification masks the original differences in fluvial landforms, making different scenarios visually more similar. Martian valley networks may have developed through a range of combinations of runoff erosion and seepage weathering, which can complicate the interpretation of the processes based on final landform morphology. Unequivocal identification of seepage involvement of valley incision on Mars may not be possible without knowledge of subsurface properties (hydraulic conductivity, layering, degree of cementation, etc.) and the grain sizes of sediment transported through the valley systems.

Citation: Luo, W., and A. D. Howard (2008), Computer simulation of the role of groundwater seepage in forming Martian valley networks, *J. Geophys. Res.*, *113*, E05002, doi:10.1029/2007JE002981.

1. Introduction

[2] The processes forming Martian valley networks (VNs) have important implications for the hydrologic cycle and associated potential for life on Mars. Theater-headed valleys on Mars, also characterized by short stubby tributaries, near constant valley width, U-shaped cross section, low drainage density, and irregular longitudinal profile, similar to those observed in Colorado plateau [*Laity and Malin*, 1985], have often been attributed to erosion by emerging groundwater (i.e., seepage erosion or groundwater sapping) rather than by surface runoff [*Sharp and Malin*, 1975; *Pieri*, 1980b; *Carr*, 1996]. This mechanism of valley formation would not necessarily require conditions much warmer than the current cold climate. However, some more recent studies using higher-resolution data have revealed the importance of fluvial surface runoff and by inference at least some precipitation on early Mars [*Craddock and Howard*, 2002; *Mangold et al.*, 2004; *Mangold and Ansan*, 2006; *Howard*, 2007]. In addition, a number of studies have cast some uncertainties on groundwater sapping as the sole mechanism for forming either terrestrial or Martian valleys with "typical" sapping characteristics [*Irwin et al.*, 2006; *Lamb et al.*, 2006]. These new developments call for careful reevaluation of the evidence that supports groundwater sapping origin of VNs. Computer simulation of landform development on Mars offers a valuable tool to explore the relative importance of groundwater versus surface water in forming Martian VNs. Previous computer modeling of groundwater sapping mostly focuses on terrestrial context [*Howard*, 1988; *Luo et al.*, 1997]. *Howard* [2007] recently used computer simulation to better understand the interplay between impact cratering and fluvial erosional processes in forming Martian highland landscapes. This paper is a natural extension of that study focusing on the interplay between surface fluvial processes and groundwater seepage processes, which has not been reported.

2. Definition of Terms

[3] In order to avoid confusion, we adopted the terminology proposed by *Dunne* [1990] and also followed by *Lamb et al.* [2006]. Weathering processes that are facilitated by emerging groundwater or seepage (e.g., salt precipitation, chemical dissolution or frost growth) are collectively referred to as seepage weathering. The removal of mass from a seepage face by exfiltrating flow is termed seepage erosion. In unconsolidated sediments, seepage erosion can occur in the absence of seepage weathering if the discharge

[1]Department of Geography, Northern Illinois University, DeKalb, Illinois, USA.
[2]Department of Environmental Sciences, University of Virginia, Charlottesville, Virginia, USA.

0148-0227/08/2007JE002981

of seepage water is sufficient to detach and mobilize the sediment. However, in rock, seepage weathering is needed to render the rock cohesionless before fluvial erosion can occur, either by seepage erosion or runoff. Sapping describes processes that undercut or undermine a scarp leading to an overhang. A variety of processes cause sapping (e.g., cut bank erosion by a meandering river, wave erosion of a sea cliff, seepage erosion at the base of a scarp or headwall, plunge pool erosion at the base of a waterfall). The term groundwater sapping then refers to sapping induced by seepage erosion.

3. Model and Its Parameterization

[4] The computer model has been developed by Howard [*Howard*, 1994, 1997, 2007; *Forsberg-Taylor et al.*, 2004]. It can simulate impact cratering, lava flows, eolian modification, and drainage basin processes, including physical or chemical weathering of rocks to form transportable colluvium, mass wasting by nonlinear creep, fluvial detachment, and fluvial transport and deposition, and groundwater sapping [*Howard*, 1994, 1997, 2007; *Forsberg-Taylor et al.*, 2004]. The model incorporates mass wasting, which at the scale of the present simulations primarily results in valley side slopes being at approximately the angle of repose for cohesionless materials. For details of how the fluvial erosion and impact cratering processes are modeled, please refer to *Howard* [1994, 2007]. Here we briefly outline the model and its parameterization, with more details on groundwater modeling.

3.1. Groundwater Flow Governing Equation

[5] Valley erosion on Earth as a result of groundwater seepage occurs in two very distinct settings, seepage erosion in unconsolidated sediments and seepage weathering of coherent rocks. Our simulation scenarios target these two terrestrial end-member cases in order to provide some insights into the Martian processes.

[6] The source of the groundwater can be as a result of nearby surface recharge, contributions from distant recharge sources as in artesian groundwater seeps, or by hydrothermally induced groundwater circulation [*Gulick and Baker*, 1989; *Gulick*, 1998]. We assume, however, water input in the model is from precipitation, which can either flow as surface runoff or infiltrate and reemerge in seeps and springs to feed surface drainage. We also assume that before the end of heavy bombardment, Martian landscape would be dominated by impact cratering. We focus on simulating the modification of the cratered terrain by surface runoff water and emerging groundwater after heavy bombardment. The model also assumes uniform bedrock material strength and does not simulate effects of layers of different strength.

[7] Groundwater flow has been included in the drainage basin model represented as unconfined, steady state DuPuit flow (vertical flow components much smaller than horizontal components). The governing equation is

$$\frac{\partial}{\partial x}\left(\left[\int_{-\infty}^{h_w} K(z)dz\right]\frac{\partial h_w}{\partial x}\right)+\frac{\partial}{\partial y}\left(\left[\int_{-\infty}^{h_w} K(z)dz\right]\frac{\partial h_w}{\partial y}\right)+I_{xy}=0, \quad (1)$$

where x and y are the horizontal axes, K is an horizontally isotropic but possibly spatially varying hydraulic conductivity that varies with elevation z, h_w is the water table elevation, and I_{xy} is recharge (due to infiltrating precipitation or hydrothermal upwelling). Hydraulic conductivity is assumed to decrease as a negative exponential function with depth from a value of K_0 at the ground surface at $z = z_s$

$$K(z) = K_0 e^{-\beta(z_s - z)}, \quad (2)$$

where β governs how rapidly hydraulic conductivity decays with depth.

[8] *Clifford and Parker* [2001], following *Manning and Ingebritsen* [1999], suggest crustal permeability declines in proportion to the logarithm of depth. However, since this functional form does not give a finite surface permeability (or hydraulic conductivity), we assume in equation (2) that hydraulic conductivity declines as a negative exponential of depth in a functional relationship similar to that proposed by *Clifford and Parker* [2001] for porosity. The model for porosity decrease proposed by *Clifford and Parker* [2001] suggests that porosity diminishes by a factor two in the first two kilometers below the surface. The scaled permeability relationship by *Clifford and Parker* [2001] suggests an even more rapid decay rate with depth, decreasing by about 1 order of magnitude between 1 and 2 km below the surface. Using hydrogeologic, thermal, seismic, and magmatic modeling constraints, *Saar and Manga* [2004] also found that for shallower depths (typically $z \leq 0.8$ km and up to $z \leq 2$ km) an exponential relationship for permeability "fits data better (at least for the Cascades and seemingly for continental crust in general)."

[9] Thus, equation (1) can be expressed in the more typical form of the DuPuit-Forsheimer equation by expressing the integral as the product of the surface hydraulic conductivity and an effective aquifer depth, h_e

$$\frac{\partial}{\partial x}\left(K_0\, h_e\,\frac{\partial h_w}{\partial x}\right)+\frac{\partial}{\partial y}\left(K_0\, h_e\,\frac{\partial h_w}{\partial y}\right)+I_{xy}=0, \quad (3)$$

where, substituting equation (2), h_e is given by

$$h_e = \frac{e^{-\beta(z_s - h_w)}}{\beta}. \quad (4)$$

This form of the equation is used in model calculations. (Note if we define an effective transmissivity T_e as $T_e = K_0\, h_e$, equation (3) takes a more standard form). The model assumes a steady state groundwater flow. The water table configuration is found by an iterative solution to the finite difference approximation of the equation, starting from a level water table at the elevation of the lowest topographic point. Initially only this lowest point is fixed head. During the iterative solution any calculated water table elevation that is higher than the surface elevation is converted to fixed head, and the solution continues until convergence to a stable water table. Figure 1d shows an example of a final water table surface. During each iteration, equation (4) must be solved for the value of h_e and the head gradients must be determined for substitution in equation (3). At fixed head locations equation (3) is solved for I_{xy}; negative values

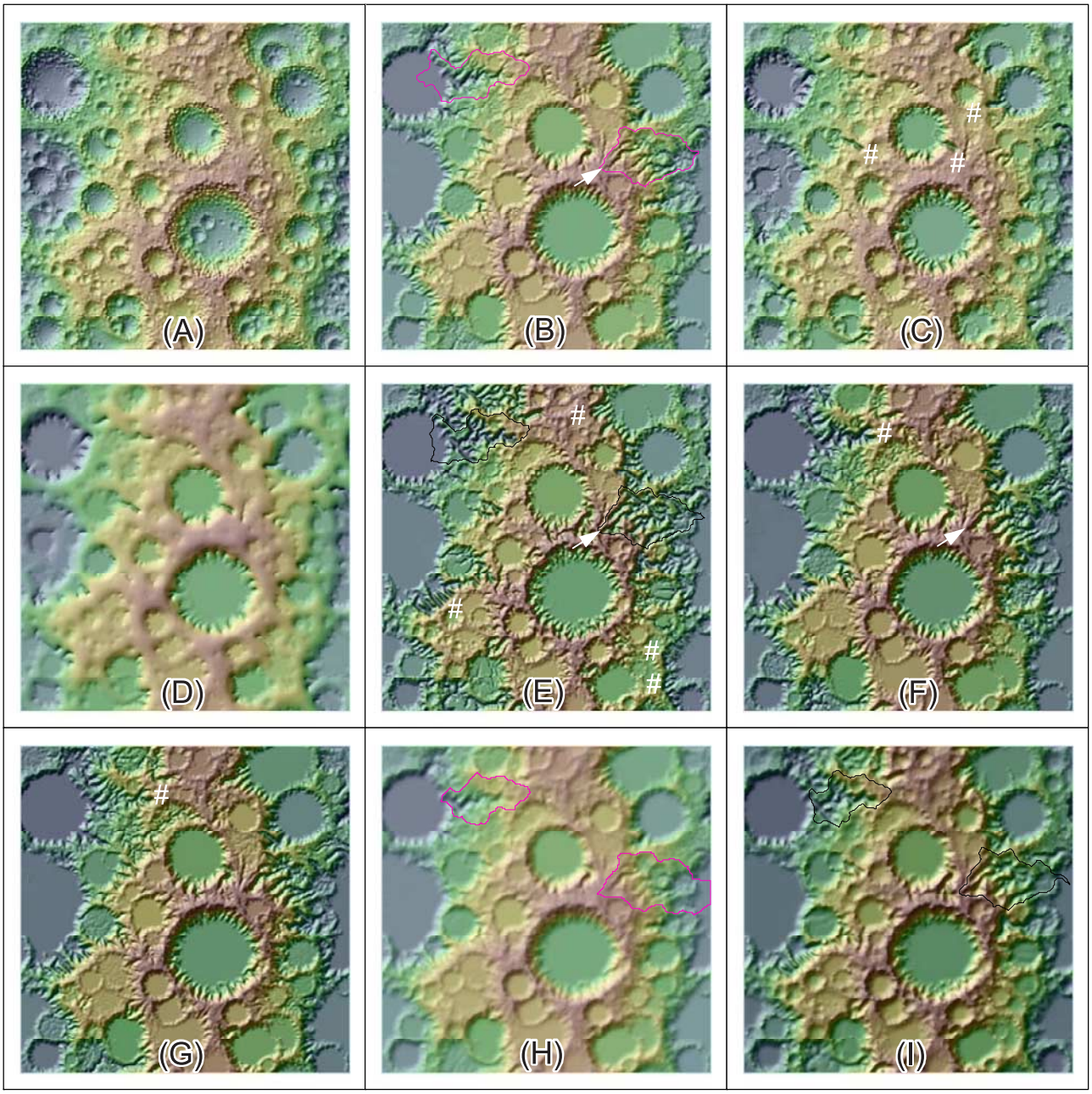

Figure 1. Shaded relief maps of simulation results. Color ramp from blue to brown indicates elevation or water table from low to high. (a) Initial conditions of simulation (a cratered terrain). (b) Erosion solely by surface water fluvial erosion (no groundwater involvement). Pink lines outline two basins whose hypsometric curves are shown in Figure 4. (c) Groundwater seepage erosion (all precipitation infiltrates into ground and seeps out as groundwater discharge that contributes to surface flow) on unconsolidated sediments (grain size diameter = 0.0002 m, recharge rate = 1 m/a, $\beta = 0.00347$) (d) Groundwater table for Figure 1c. (e) Same as for Figure 1c except $\beta = 0.00693$. Black lines outline two basins whose hypsometric curves are shown in Figure 4. (f) Seepage weathering on bedrock with negligible groundwater contribution to surface flow, but groundwater seepage causes accelerated weathering of bed rock ($W_s = 0.002$). Fluvial erosion erosion uses same conditions as in Figure 1b. (g) Same as for Figure 1f except $W_s = 0.001$. (h) Eolian modification of Figure 1b. Pink lines outline two basins whose hypsometric curves are shown in Figure 4. (i) Eolian modification of Figure 1e. Black lines outline two basins whose hypsometric curves are shown in Figure 4.

imply water discharged to the surface. This discharge is routed downstream, adding to surface flow from runoff.

3.2. Seepage Erosion in Unconsolidated Sediment

[10] Direct entrainment and transport of sediment by seepage occurs in the classic cases of beach erosion during falling tides [e.g., *Higgins*, 1984; *Otvos*, 1999] and on noncohesive river banks during falling river stages [e.g., *Budhu and Gobin*, 1995]. Seepage erosion has been implicated in the erosion and maintenance of channel heads [e.g., *Dunne*, 1980, 1990; *Higgins*, 1982, 1984; *Schumm and Phillips*, 1986; *Montgomery and Dietrich*, 1989; *Coelho Netto and Fernandes*, 1990; *Teixeira De Oliveira*, 1990; *Gehrels and Van De Plassche*, 1992; *Uchupi and Oldale*, 1994; *Schumm et al.*, 1995; *Nash*, 1996; *Gabbard et al.*, 1998; *Spence and Sauchyn*, 1999; *Gutierrez et al.*, 2003; *Froede and Williams*, 2004]. Theory and laboratory experiments in fine-grained cohesionless sediment demonstrate the ability of seepage flow to excavate valleys [*Kochel et al.*, 1985, 1988; *Howard*, 1988; *Howard and McLane*, 1988; *Gomez and Mullen*, 1992; *Lobkovsky et al.*, 2004; *Shorghofer et al.*, 2004; *Ni and Capart*, 2006]. Emergent groundwater fluxes sufficient to erode and transport sediment depend upon source deposit grain sizes small enough to be transported (generally finer than gravel) and large enough to support sufficient groundwater flow (generally sand size or larger). Groundwater contributions to valley erosion can also occur in fine-grained cohesive sediment through hydraulic erosion and slaking by flow through discrete subsurface openings ("piping" [e.g., *Jones*, 1971, 1987; *Nwankwor et al.*, 1998; *Tomlinson and Vaid*, 2000; *Onda*, 2002]).

[11] We consider only erosion of cohesionless sediment in the direct erosion and transport and assume subsurface deposits with a surface hydraulic conductivity, K_0, of about 0.31×10^{-5} m s^{-1} (equivalent to silty to clean sands [*Freeze and Cherry*, 1979]) and a generous recharge (1 m/a, where a is years). This combination of parameters allows sufficient emergent groundwater flux to be able to erode sand-sized particles. As discussed by *Howard and McLane* [1988], the erosion of cohesionless sediment by emergent groundwater is largely regulated by the ability of the fluvial flows to remove sediment from the stream head and direct sediment destabilization by seepage is restricted to a very narrow zone. As a result, in these simulations we do not include any special process within seepage channels over and above normal fluvial transport in response to the total discharge of water resulting from groundwater discharge.

[12] All rainfall on unsaturated uplands is assumed to infiltrate and to eventually reemerge in seepage locations and contribute to total runoff. All rainfall on saturated locations with effluent groundwater, however, is assumed to contribute to total runoff (in addition to the groundwater seepage contribution). In these simulations the bed material is assumed to be sand with a grain size of 0.2 mm. Two simulations are reported here, one with the hydraulic conductivity decay constant, $\beta = 0.00347$ (hydraulic conductivity decreases to half its surface value 200 m below the surface) and $\beta = 0.00693$ (half value at 100 m depth).

[13] For the erosion of unconsolidated sediment, we assume that no weathering occurs to the sediment prior to erosion, which, in the simulation model, is equivalent to an infinite thickness of regolith.

3.3. Seepage Erosion by Bedrock Weathering

[14] The second case of enhanced weathering of rock at zones of emergent seepage targets development of canyons in permeable bedrock through weakening and undermining of the rock in canyon headwalls, as proposed for some canyons developed in the Navajo Sandstone Formation of the southwestern United States [e.g., *Laity*, 1983; *Laity and Malin*, 1985; *Howard and Kochel*, 1988; *Howard and Selby*, 1994]. Although *Laity and Malin* [1985] suggest that emergent seepage may directly erode the mass-wasted wall rock, *Howard and Kochel* [1988] and *Lamb et al.* [2006] argue that surface flows from seepage are insufficient to remove even sand-sized debris and that direct surface runoff is responsible for removal of sapping debris (although additional size reduction of mass wasting debris may occur because of weathering by seepage). Accordingly, we assume that the role of emergent groundwater is primarily to provide enhanced weathering to enhance erosion of bedrock by runoff. We target our simulations to canyon erosion in materials with properties similar to the Navajo Sandstone. Hydraulic conductivity of the Navajo Sandstone varies widely because of differences in porosity, cementing, and fracture density. Estimated values range over several orders of magnitude, from about 1×10^{-7} to 1×10^{-4} m/s, with typical averages about 2×10^{-6} m/s [e.g., *Brown and Eychaner*, 1988; *Heilweil et al.*, 2000, 2007; *Thomas*, 2002]. In the Navajo Sandstone, seepage often occurs from minor exposed aquicludes or above the shaly layers at the contact between the Navajo and the underlying Kayenta Formation. To compensate for the lack of aquicludes in the model, we assume a fairly small hydraulic conductivity of 1.2×10^{-7} m/s to give high groundwater levels for reasonable recharge rates. Recharge rates into the Navajo Sandstone typically range from 0.005 to 0.05 m/a, averaging about 0.02 m/a [*Zhu*, 2000; *Heilweil et al.*, 2007]. These recharge rates correspond to about 10% of yearly precipitation. Again, to produce relatively high groundwater levels in our simulations, we assume a recharge rate near the high end of the observed spectrum, 0.04 m/a.

[15] The mechanisms by which seepage reduces rock strength are uncertain and not quantified. Crystal growth, cement dissolution, biotic activity on the seepage face (typically vegetated), and freeze-thaw are possible processes [*Laity*, 1983; *Howard and Kochel*, 1988]. Despite the process uncertainty, seepage faces nearly universally occur at the deepest part of valley headwall alcoves, indicating a positive relationship between bedrock erosion and occurrence of seepage. Scarp retreat through seepage weathering was simulated by *Howard* [1995] with the assumption that the rate of scarp retreat was proportional to a power law relationship to seepage specific discharge. These simulations demonstrated that scarp retreat in proportion to seepage specific discharge is sufficient to create canyons with nearly constant width, rounded headwalls, and stubby branching of the type observed in canyons in the Navajo Sandstone characterized by seepage alcoves. In the present simulations we assume that the bedrock weathering rate, $\dot{z}_b$ (m/a), is enhanced in proportion to the seepage flux

divergence, I_{xy} (m/a), which quantifies the seepage specific discharge to the surface

$$\dot{z}_b = W_0 e^{-\omega H} + W_s I_{xy}, \tag{5}$$

where H is regolith thickness (m), W_0 is the background weathering rate (m/a), and W_s is the rate of weathering induced by groundwater seepage. In the absence of applicable theory or quantitative measurements, we have adopted a simple linear relationship as test of the efficacy of seepage weathering to affect the course of fluvial erosion. We assume $\omega = 0.03$ m^{-1}, $W_0 = 0.0001$ m/a, and $W_s = 0.002$ for the nominal case. The small value of the background weathering rate, W_0, means that weathering will be very slow except in locations with emergent seepage. Erosion by surface discharge is parameterized as a function of direct runoff using the same process formulation as the case of pure runoff erosion (see below). For this case seepage flows make a negligible contribution to total surface flows.

3.4. Runoff Erosion Model

[16] The landscape model, used in the simulations reported here, is essentially the DELIM model as reported by *Howard* [1994, 1997, 2007] and *Forsberg-Taylor et al.* [2004] with components modeling physical or chemical weathering of rocks to form transportable colluvium, mass wasting by nonlinear creep, fluvial detachment, and fluvial transport and deposition. Parameters used for these simulations are based upon terrestrial values in semiarid or arid landscapes except for correcting for the difference in gravity between Mars and Earth. We briefly outline the model below, and additional background and model details can be found by *Howard* [1994, 1997, 2007].

[17] It is assumed that the materials below the surface (lava, sediments, ejecta, etc., collectively termed ''bedrock'') may be indurated, but can be weathered at a finite rate by physical or chemical processes to form colluvium. The rate of bedrock weathering is given by equation (5) with the seepage weathering term, W_s, set to zero. Note that $\dot{z}_b$ is the rate of lowering of the colluvial bedrock contact, and when weathering is isovolumetric, as is assumed here, it does not change the land surface elevation.

[18] The potential rate of erosion by mass wasting, $\dot{z}_m$, is proportional to the spatial divergence of colluvial mass flux, $\boldsymbol{q_m}$

$$\dot{z}_m = -\nabla \cdot \boldsymbol{q_m}. \tag{6}$$

Colluvial flux is given by a nonlinear relationship

$$\boldsymbol{q_m} = \left[K_s |S| + K_t \left(\frac{1}{1 - \{|S|/S_t\}^a} - 1 \right) \right] \boldsymbol{s}, \tag{7}$$

where $|S|$ is the absolute value of local slope, $\boldsymbol{s}$ is the unit vector in the downslope direction, a is an exponent with an assumed value of 3.0, S_t is a threshold gradient at which the rate of mass wasting becomes infinite (i.e., landsliding), and K_s is creep diffusivity. K_t takes a value (0.5) that provides for a smooth but rapid approach to threshold slopes for rapid rates of erosion. Erosion of bare bedrock slopes (exposed when rates of erosion are greater than the maximum weathering rate given by equation (5)) follows equation (7), but with K_s set to zero and a steeper critical gradient, S_t, of 2.7. Erosion of bedrock slopes involves a wide variety of processes and resultant forms [e.g., *Howard and Selby*, 1994]), and the assumed critical gradient (about 70°) is chosen to represent bedrock slopes in rapidly incising canyons.

[19] Because of the large cell size in the simulations discussed below (400 m) mass transport by linear creep (K_s in equation (7)) and the shape of small slopes is not well characterized. Longer slopes in rapidly eroding locations (e.g., on crater rims), however, tend to be close to the threshold gradient (0.8).

[20] In the present modeling potential erosion by fluvial detachment, $\dot{z}_f$ in bedrock and regolith-floored channels and on steep slopes where the flow is carrying less than a capacity load is assumed to be proportional to the shear stress, τ, exerted by flowing water

$$\dot{z}_f = -K_f(\tau - \tau_c), \tag{8}$$

where K_f is a parameter with units m^2 a kg^{-1}. The critical shear stress, τ_c, is assumed to be zero in the present simulations. Assuming that the reference shear stress is that which corresponds to the mean annual flood, the value of K_f that we assume (0.0001 m^2 a kg^{-1}) corresponds to terrestrial rates of erosion in moderately strong sedimentary rocks. For the case of direct seepage erosion we assume a weaker substrate with $K_f = 0.01$ m^2 a kg^{-1}.

[21] Flow of water is assumed to be channelized and originating from runoff. Shear stress can be related to channel gradient and drainage area using equations of hydraulic geometry and steady, uniform flow as discussed by *Howard* [1994, 2007]

$$\tau = \rho_f g R S, \tag{9}$$

$$V = K_n g^{1/2} R^{2/3} S^{1/2} / N, \tag{10}$$

$$Q = RWV, \tag{11}$$

$$Q = PA^e, \tag{12}$$

$$W = K_w Q^b, \tag{13}$$

where R is hydraulic radius, S is channel gradient, V is mean velocity, N is Manning's resistance coefficient, P is a specific runoff yield (depth per unit area per unit time), Q is an effective discharge, W is channel width, A is drainage area, and K_n, K_p, K_a, K_w are coefficients. Channel width, as parameterized in equation (13), is generally much less than the size of an individual grid cell, and following *Howard* [1994], each grid cell is assumed to host a single channel that carries the total discharge through that cell. The coefficients and exponents in equations (9)–(13) are assumed temporally and spatially invariant. The following parameter values are assumed: $N = 0.03$, $K_n = 0.3$ (for

metric units); $P = 3.5 \times 10^{-7}$ m/s, $e = 1.0$, $b = 0.5$, and $K_w = 5.0$ $s^{0.5}$ $m^{-0.5}$.

[22] Regolith is assumed to be more erodible than the bedrock by a factor $M = 10.0$, which is assumed to influence the bed erodibility and the threshold of erosion; thus, the potential rate of fluvial erosion of channels flowing on regolith, $\dot{z}_r$, is calculated from equation (8) by multiplying K_f by M and dividing τ_c by M.

[23] When the flux of sediment transported as bed and suspended load reaches or exceeds the transporting capacity of the flow (an alluvial channel as opposed to a bedrock channel), the rate of erosion or deposition, $\dot{z}_f$, is proportional to the spatial divergence of transport flux $\boldsymbol{q_s}$ (volume per unit time per unit width)

$$\dot{z}_f = -\nabla \cdot \boldsymbol{q_s} \tag{14}$$

[24] Sediment transport flux is estimated using a bed load transport formula that expressed as the relationship between a dimensionless transport rate, Φ, and a dimensionless shear stress, τ^*

$$\Phi = K_e\left\{\tau^* - \tau_c^*\right\}^p, \tag{15}$$

where

$$\Phi = \frac{q_{sb}(1-\mu)}{g^{1/2}\, d^{3/2}(S_s-1)^{1/2}} \tag{16a}$$

and

$$\tau^* = \frac{\tau}{\rho_f g(S_s-1)d}. \tag{16b}$$

[25] In these equations τ^*_c is the value of τ^* at the threshold of motion, q_{sb} is bed sediment transport rate in bulk volume of sediment per unit time per unit channel width, S_s is the specific gravity of the sediment, g is gravitational acceleration, ρ_f is the fluid density, d is the sediment grain size, and μ is alluvium porosity. We assume a sand bed with $d = 0.0002$ m, $K_e = 40.0$, and $p = 1.5$. For all simulations $\tau^*_c = 0.05$, and $S_s = 2.65$ and $\mu = 0.5$. The shear stress is estimated from equations (9)–(13), with the dominant discharge for sediment transport assumed to be 0.6 of the mean annual flood, flowing 3% of the year. However, for the seepage erosion simulations (section 3.2) we assume that the dominant discharge is that from groundwater discharge and that the flow is constant (100% of the year). Rivers vary from those transporting dominantly suspended load to those carrying primarily bed load [e.g., *Schumm*, 1977]. In the absence of information for Martian channels, bed sediment load is assumed to constitute 20% of sediment eroded from slopes.

3.5. Eolian Modification Model

[26] Eolian modification is based upon an exposure index, I_e, which is based upon a weighted sum of the gradients, S_i, between the local elevation, E, and that of a surrounding location, E_i

$$S_i = [(E_i - E)/\Delta x_i], \tag{17}$$

where Δx_i is the distance to the nearby point [*Forsberg-Taylor et al.*, 2004]. The exposure index, I_{ek}, for points lying along a transect, k, extending from the given location is given by

$$I_{ek} = \sum_{i=1}^{n} S_i\, e^{-\eta \Delta x_i} \Big/ \sum_{i=1}^{n} e^{-\eta \Delta x_i}, \tag{18}$$

where the parameter η governs the relative importance of nearby versus distant points in determining the exposure [*Forsberg-Taylor et al.*, 2004]. Points that are not visible from the location (lying behind a closer high point) are not included. For computational efficiency exposure indices are calculated only along the eight cardinal and diagonal directions from a given point and the net exposure index, I_e, is the average of the eight I_{ek}. The rate of eolian erosion or deposition, $\partial z/\partial t|_e$ is a function of the exposure index. We used the same functional dependence of eolian erosion on exposure index as illustrated in Figure 3 of *Forsberg-Taylor et al.* [2004]. Eolian erosion and deposition need not occur simultaneously. Deposition can occur from a nearly still atmosphere, whenever dust loading occurs from dust storms, crater impacts, or volcanic eruptions. Erosion occurs on exposed areas during strong wind events. Further description of the eolian model is presented by *Forsberg-Taylor et al.* [2004].

4. Results

[27] For easy comparison and better understanding of the processes, we first present the simulations starting with the same initial cratered terrain as shown in Figure 1a and we will then briefly discuss the result with a different initial condition. The grid size is 256 by 256 with each cell having a dimension of 400 by 400 m. The whole simulation domain has dimension of about 102 by 102 km. All scenarios were run for 2500 iterations, which roughly correspond to a minimum of 2.5 million years on the basis of terrestrial process rate scaling in arid to semiarid climates. We now describe the result of each scenario in more detail.

[28] The simulations have been conducted to examine whether groundwater involvement in fluvial erosion imparts distinctive morphology to the resulting landscape. It has long been postulated that the signature morphology of groundwater erosional processes are sparse, weakly branched, box canyons with abrupt, theater-shaped headwalls [e.g., *Higgins*, 1982, 1984; *Laity and Malin*, 1985; *Howard and Kochel*, 1988]. Our simulations of groundwater involvement in erosion of cratered landscapes tend to confirm this signature morphology.

4.1. Surface Discharge Solely From Runoff

[29] Erosion dominated by runoff erosion produces landscapes with fairly uniform intensity of dissection on upland slopes, strongly dendritic valley networks, and narrow valleys that gradually shallow headward (Figure 1b), typical of fluvially eroded landscapes. Additional examples of runoff erosion of cratered surfaces are presented by *Howard* [2007] for a variety of hydrologic scenarios and for some simulations with concomitant impact cratering. The fluvially dominated simulation in Figure 1b assumes a dominantly weathering-limited landscape with a relatively

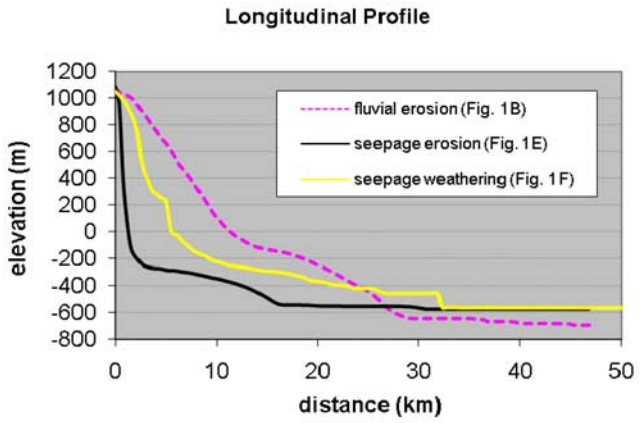

Figure 2. Longitudinal profiles of the valley networks pointed by white arrow in Figures 1b, 1e, and 1f.

slow rock weathering rate (0.0001 m/a) and it serves as a process comparison to the two scenarios of seepage-related erosion. The longitudinal profile of a valley started at the location pointed by the white arrow is shown in Figure 2, which is a concave upward profile typical of fluvial erosion.

4.2. Seepage Erosion in Unconsolidated Sediments

[30] Direct erosion by groundwater seepage is possible in fine-grained cohesionless sediment as, for example, the small valleys excavated on beaches during falling tides. Under this scenario, we assume that impact cratering at the end of heavy bombardment has created unconsolidated, cohesionless sediments (megaregolith) covering at least some areas of Mars, which can be subject to seepage groundwater erosion.

4.2.1. Case 1: Deep Effective Aquifer Depth (h_e = 200 m, β = 0.00347)

[31] Our simulations assumed a subsurface material characterized by a hydraulic conductivity typical of sand (0.31×10^{-5} m/s) and a recharge of 1.0 m/a. The simulation shown in Figure 1c assumes that hydraulic conductivity decreases as a negative exponential of depth beneath the surface (equation (2)), decreasing to half its surface value at a depth of 200 m. With this simulation, about 12% of the land surface initially experienced groundwater seepage to the surface, increasing to about 18% by the end of the simulation. Figure 1d shows the configuration of the water table at the close of the simulation. During the simulation, short stubby valleys formed along the lower interior walls of large impact craters (e.g., the large crater in the center of Figure 1c) and a few unbranched, short, flat-floored canyons eroded from low areas toward major groundwater divides (e.g., near "the number sign" in Figure 1c). Even with the high recharge rate and high hydraulic conductivity, fluvial erosion had essentially ceased by the end of the simulation, because the low-gradient fluvial valleys that developed lowered the water table and reduced seepage flux rates to the point that sand could no longer be transported with available discharge.

4.2.2. Case 2: Shallow Effective Aquifer Depth (h_e = 100 m, β = 0.00693)

[32] A second simulation with the same material properties and recharge rate was conducted, but with the value of β in equation (2) doubled relative to the previous simulation such that the hydraulic conductivity decreased to half the surface value at a depth of 100 m (Figure 1e). This has the effect of decreasing the effective aquifer depth, h_e, in equation (4), increasing hydraulic gradients, and increasing the fraction of the land surface with seepage efflux (42% initially, decreasing at the end of the simulation to about 19% as the eroded valleys lowered the water table and captured most of the seepage).

[33] Under this set of conditions valley incision was initiated at the base of a slope or crater wall and worked its way headward but rarely reached close to the drainage divides. The longitudinal profile of a valley pointed by white arrow in Figure 1e clearly demonstrated this feature (Figure 2). In comparison with the longitudinal profile from solely fluvial erosion, the seepage erosion generated valley is steeper at the head because of the headward erosion. Valley deepening and extension occurred throughout the simulation, producing low-gradient, wide, stubby valleys with weak branching with an overall pattern similar to that resulting from seepage weathering in Figure 1f. In addition to the abrupt valley headwalls, a diagnostic feature of seepage erosion of cratered landscapes is the scattered occurrence of nearly parallel flat-floored drainages terminating at similar positions on regional slopes, as in the locations marked with the number sign in Figure 1e.

[34] Simulation runs with same parameters as above but increasing sediment grain size to fine gravel result in no channel development (not shown), which suggest that the role of direct seepage erosion is probably limited on Mars.

4.3. Seepage Weathering of Bed Rock

[35] Under this scenario, groundwater seeps out to the surface and causes accelerated weathering of the bedrock, which is then more easily removed by fluvial processes. This scenario targets the type of groundwater involvement in canyon development in indurated sandstones, particularly the Navajo Sandstone of the Colorado Plateau, USA. As discussed earlier, values of hydraulic conductivity and recharge rates are representative of the Navajo Sandstone aquifer. Removal of seepage-weathered sediment is assumed to occur by fluvial erosion dominated by discharge from direct runoff.

4.3.1. Case 1: Strong Contribution of Seepage Weathering (W_s = 0.002)

[36] This simulation assumes a large seepage component of weathering, W_s in equation (5) of 0.002. The concentrated weathering in zones of seepage results in the expected morphology of sparse, weakly branched, deep canyons with abrupt headwalls (e.g., the canyon to left of the number sign in Figure 1f), although some background fluvial erosion occurs without seepage involvement. The steep slope of headwalls can also be seen in profile (Figure 2) of the valley pointed by the white arrow in Figure 1f. The comparison with the Colorado Plateau archetype assumes that the seepage weathering, although in the natural setting involving weakening of a thin seepage face, undermines the overlying rock (groundwater sapping), causing rockfalls that pulverize much of the sandstone. Seepage may, in addition, further weather the fallen debris [see, e.g., *Laity and Malin*, 1985; *Howard and Kochel*, 1988]. In the

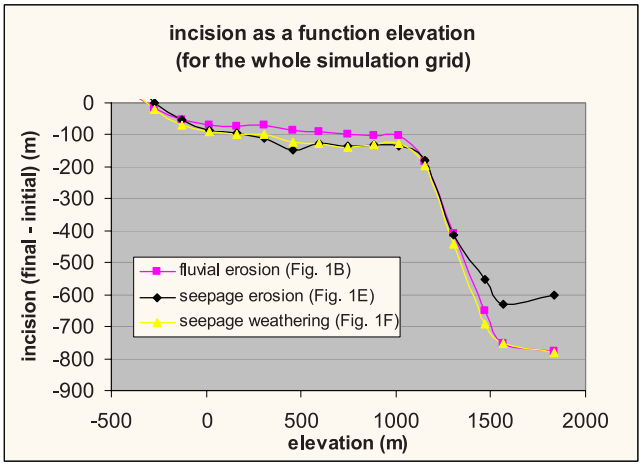

Figure 3. Distribution of incision as a function of elevation for Figures 1b, 1e, and 1f for the whole simulation grid. Incision is defined as final topography minus initial topography (more negative value indicates deeper incision).

Colorado Plateau setting removal of debris produced by seepage weathering is dominated by direct runoff from precipitation [*Howard and Kochel*, 1988; *Lamb et al.*, 2006]. Discharge directly from seepage from sandstones with hydraulic conductivities and recharge rates characteristic of the Navajo Sandstone is insufficient to transport even sand-size sediment [*Lamb et al.*, 2006]. To confirm this, a simulation run (not shown) using the same parameters as those in Figure 1f but with the surface water discharge being solely from groundwater seepage resulted in no fluvial erosion.

4.3.2. Case 2: Varying Relative Contribution of Seepage Weathering (W_s = 0.001)

[37] A set of simulations were conducted with reduced values of the seepage weathering coefficient, W_s. One such simulation is shown in Figure 1g. As would be expected, the resulting pattern of fluvial incision was transitional between the strong seepage weathering in Case 1 (Figure 1f) and the solely runoff erosion case in Figure 1b. With a small W_s, the valleys are small and shallow, whereas a large W_s leads to bigger and deeper valleys that looks more like typical groundwater sapping valleys (compare the valley to left of the number sign in Figures 1f and 1g). So depending on the seepage weathering rate, different degree of dissection can be generated through seepage weathering.

4.4. Comparing Incision as a Function of Elevation

[38] To illustrate the channel incision as a function of elevation for different scenarios, we did the following calculation for fluvial erosion (Figure 1b), seepage erosion (Figure 1e), and seepage weathering (Figure 1f): (1) com-

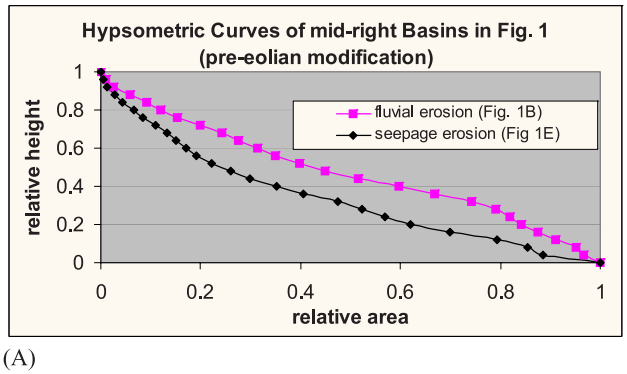

(A)

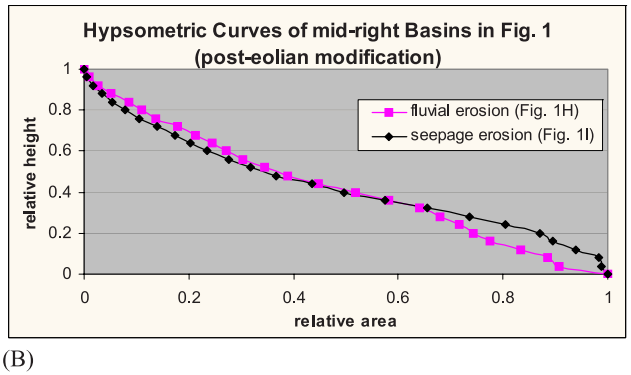

(B)

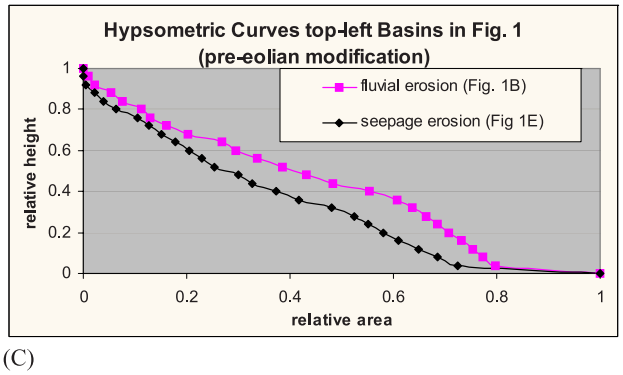

(C)

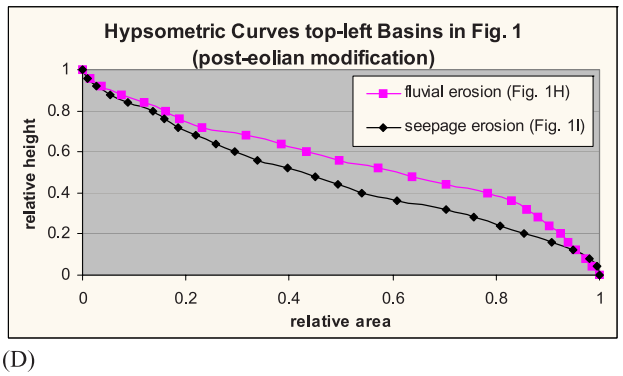

(D)

Figure 4. Hypsometric curve of the basin as outlined in Figures 1b, 1e, 1h, and 1i. Relative area is the area at a given elevation relative to the total area. Relative elevation is the elevation relative to the total relief of the basin. (a) Preeolian modification for the two midright basins. (b) Posteolian modification for the two midright basins. (c) Preeolian modification for the two top-left basins. (d) Posteolian modification for the two top-left basins.

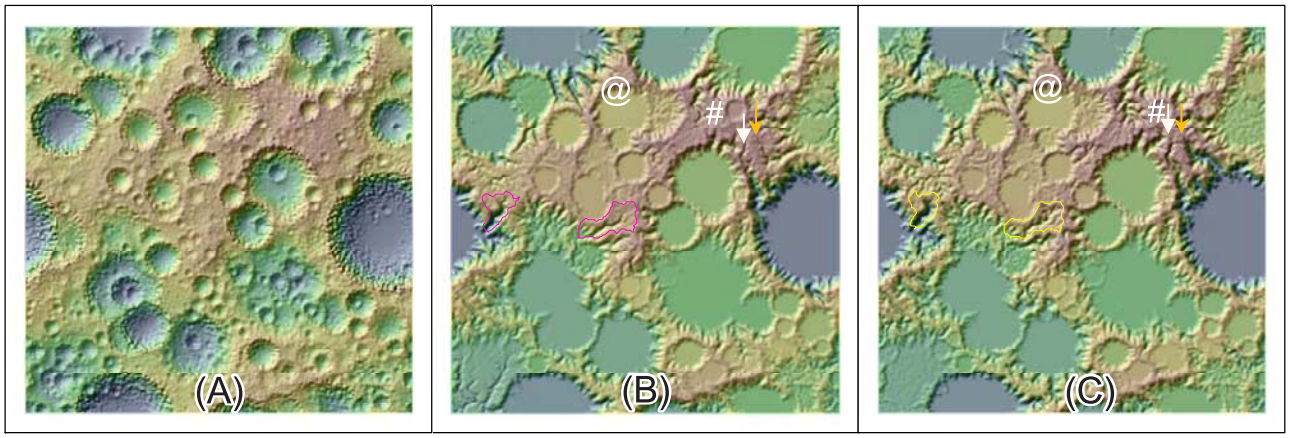

Figure 5. Simulation result from a different initial topographic condition. Color ramp from blue to brown indicates elevation from low to high. (a) initial topography, (b) fluvial erosion (using same parameter values as in Figure 1b), and (c) seepage weathering (using same parameter values as in Figure 1f).

pute the difference between the final topography and initial topography (negative values indicate incision); (2) divide the initial topography into 25 equal elevation zones; (3) calculated the average of the difference (or incision from calculation 1 within each zone (from calculation 2)); and (4) plot the average of incision in each zone as function of the zone elevation. The result is shown in Figure 3. For fluvial erosion there is smaller incision than seepage erosion and seepage weathering at lower elevation. At higher elevation, however, incision caused by fluvial erosion is similar to that by seepage weathering, because there is not much seepage at higher elevation anyway, and thus the erosion there is primarily due to regular fluvial erosion, which explains the similar incision there. For seepage erosion, again there is not much seepage at higher elevation, so the incision there is lower than the other two cases.

4.5. Eolian Modification

[39] In order to test the effect of eolian modification on valley network morphology, we used the end result of fluvial erosion (Figure 1b) and seepage erosion (Figure 1e) as initial conditions and run eolian processes on them. The results are shown in Figures 1h and 1i. Comparing with Figures 1b and 1e, eolian processes smooth the landscape and make them look more similar. The sharply defined channels in Figures 1b and 1e are now shallower and more rounded. The short channels developed on the crater walls are also smoothed out. We also obtained the hypsometric curves of the basins outline in the figures (one located in the midright of the figure and the other top-left) and compared with their preeolian counterparts (Figure 4). In the preeolian situation, the difference primarily reflects the headward erosion, similar to the longitudinal profile shown in Figure 2. However, eolian modification made these two curves more similar. This is especially the case for the midright basins (Figures 4a and 4b). The more difference for the top-left basins may be an artifact of the preeolian basins including parts of the flat area of the crater. In any case, this suggests that postformation modification may complicate the interpretation of the origin of valley networks.

4.6. Different Initial Conditions

[40] Simulation runs with different initial conditions resulted in generally similar landform patterns. One such example is shown in Figure 5. The total relief (difference of maximum and minimum elevations) of the initial topography (Figure 5a) is about 3.2 km, similar to that of Figure 1a (3.6 km). For the fluvial erosion result (Figure 5b) and seepage weathering result (Figure 5c), we used the exact same parameter values as the corresponding cases shown in Figures 1b and 1f (i.e., the only difference is the initial topography), respectively. In Figure 5b, we observe a typical fluvial channel west of the number sign draining north that starts small and increases downstream with increasing contributing area. In comparison, in the seepage weathering case shown Figure 5c, we see headward erosion created more stubby-looking channels surrounding the highland area marked by the number sign and steeper and bigger valley heads near "the at symbol" and in the basin near the west edge of the figure. It is interesting to note that headward erosion has caused the channel pointed by the orange arrow draining into the big crater (Figure 5c) to

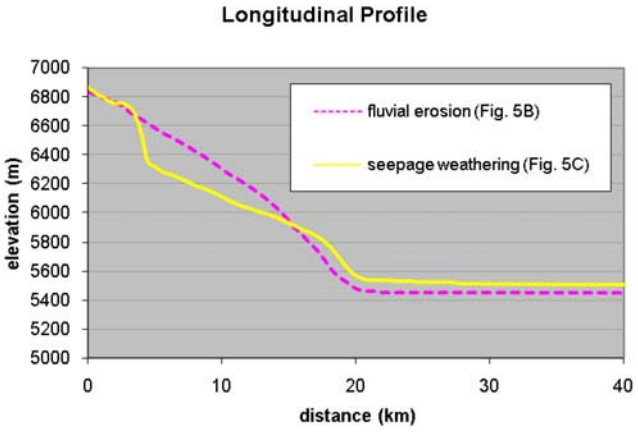

Figure 6. Longitudinal profile of channel pointed by the white arrow in Figures 5b and 5c.

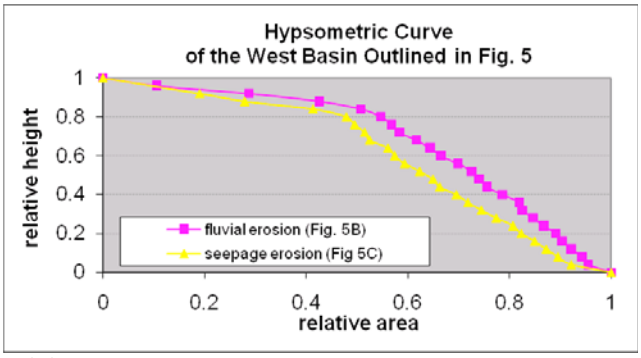

(A)

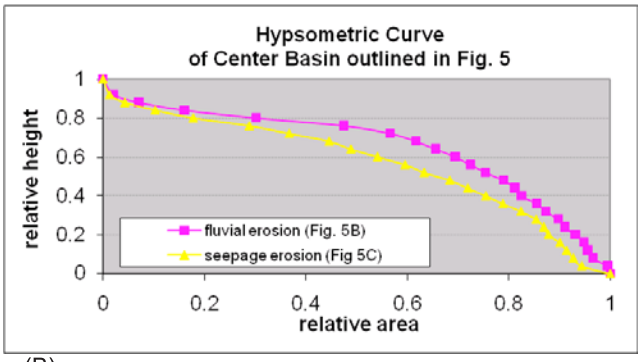

(B)

Figure 7. Hypsometric curve of the basin outlined in Figure 5 (the (a) west basin and (b) center basin).

pirate another channel that was originally draining to the northeast and shaped like the letter "L" (compare the channel pointed by orange arrow in Figure 5b). The effect of headward erosion can be seen more clearly in the longitudinal profiles of channels pointed by white arrows (Figure 6): at highest elevation, there is not much difference between seepage weathering and fluvial erosion, but between about 5900 and 6600 m, headward erosion in seepage weathering caused more erosion and steeper slope than fluvial case. This general pattern is consistent with observation made in Figures 2 and 3. The hypsometric curves of the outlined basins in Figure 5 are shown in Figure 7. These curves are similar to those in Figures 4a and 4c with seepage weathering having more overall erosion than the fluvial case. These hypsometric curves (Figures 4a, 4c, 7a, and 7b) all show more erosion for cases with groundwater involvement (seepage erosion or seepage weathering). However, the hypsometric curve of a typical groundwater sapping basin in Colorado Plateau is often seen less eroded than a typical fluvial basin [e.g., see *Luo*, 2000, Figure 4]. We interpret this as being due to the initial cratered topography used in the simulation, as opposed to a nearly planar, sandstone-capped plateau as initial topography for the Colorado Plateau, which could allow more areas subject to groundwater seepage and thus causing more headward erosion. In summary, the overall simulation results and morphometric attributes do not change with different initial condition.

5. Discussion

[41] We use a computer model to simulate the role of groundwater in forming Martian valley networks in two ways: (1) groundwater discharge contributes to surface water runoff, which causes additional erosion of unconsolidated sediments (seepage erosion) and (2) groundwater seepage causes accelerated weathering of bedrock, which makes its subsequent erosion and removal easier (seepage weathering). Simulations of both seepage weathering of indurated sediment and seepage erosion of fine cohesionless sediment produce valley networks that bear a distinctive morphology of being flat floored, weakly branched, low gradient, and ending in steep theater headwalls (e.g., Figures 1e and 1f). This morphology has long been cited as being characteristic of groundwater involvement in valley network development, both in terrestrial settings [*Laity and Malin*, 1985; *Kochel and Piper*, 1986; *Howard and Kochel*, 1988] and on Mars [*Pieri*, 1980a, 1980b; *Higgins*, 1982; *Carr*, 1995, 2002; *Malin and Carr*, 1999; *Grant*, 2000; *Malin and Edgett*, 2000; *Grant and Parker*, 2002]. The reason for the similarity between valleys produced by seepage erosion and those resulting from seepage weathering is that sediment transport is a positive function of groundwater-derived surface water flow rate, and, likewise, we assume that seepage weathering is also a positive function of seepage efflux.

[42] A number of issues complicate using valley network morphology to infer process scenarios on Mars. The numbered paragraphs below briefly summarize cautions in interpretation of valley network origin raised by *Lamb et al.* [2006].

[43] 1. Mass wasting, impact gardening [*Hartmann et al.*, 2001], and eolian infilling of valleys (e.g., compare Figures 1e and 1i) have so modified Martian valley networks that characteristic landforms such as seepage alcoves would not have survived to the present. Small headwater tributaries may have been destroyed, giving the appearance of low drainage densities and abrupt headward terminations of valley networks even if the drainage density were initially high and valleys extended close to divides.

[44] 2. Valleys with abrupt, theater-like headwalls might also be created by layered stratigraphy, such as erosion through indurated rocks (e.g., basalt flows) into underlying weak sediment (e.g., megaregolith, volcanic ash, or unconsolidated sediment). Formation of duricrusts and subsequent erosion through the crusts are an additional possibility [*Howard et al.*, 2005].

[45] 3. Fluvial erosion through layered stratigraphy followed by modification by mass wasting can produce theater-headed valley terminations [*Howard*, 1995; *Lamb et al.*, 2006].

[46] 4. Some terrestrial theater-headed valley systems previously attributed to groundwater erosion, such as Hawaiian valleys [*Kochel and Piper*, 1986] and box canyons eroded into lava flows in Idaho, may instead be formed by plunge pool erosion [*Lamb et al.*, 2006, 2007].

[47] Although the present simulations of groundwater involvement in valley development produce characteristic

valley morphology that has long been attributed to seepage processes, caution in interpretation should also be exercised because of the restrictive material and process scenarios necessary for appreciable groundwater contribution to erosion. Direct erosion solely by groundwater seepage requires subsurface materials with hydraulic conductivity at least equal to that of cohesionless fine sand and high recharge rates. Impact gardening might produce a megaregolith with appropriate hydraulic conductivity [*Clifford*, 1993; *Clifford and Parker*, 2001]. In addition, however, the presence of an appreciable fraction of gravel or larger particles within the substrate will produce a lag concentrate in valleys that seepage discharges cannot transport. In such circumstances erosion can continue only if weathering processes comminute the large particles or if occasional direct runoff aids removal of large particles. Such a process mix of seepage undermining and runoff erosion is common in terrestrial valley networks [e.g., *Schumm and Phillips*, 1986].

[48] Enhancement of valley incision by seepage weathering also requires specific substrate properties and weathering processes that may be restrictive. The subsurface aquifer must be thick, relatively massive, and it must have appreciable hydraulic conductivity coupled with cementation sufficient to sustain canyon walls while being susceptible to seepage weathering processes. Aquicludes may help to create seepage faces on valley walls. Even in the sandstones of the Colorado Plateau this set of characteristics is rare, for other thick sandstones, like the Wingate Formation and the Coconino Sandstone rarely exhibit valleys with seepage alcoves.

[49] *Lamb et al.* [2006] make the general observation that processes involved in seepage weathering are uncertain even for Earth, making extrapolation to Mars problematic. If seepage weathering occurs primarily by freeze-thaw or by crystal growth within seepage faces, then similar settings may have occurred on early Mars. But if seepage weathering on Earth is dominated by processes related to the nearly universal covering of seepage faces by biotic crusts and vegetation, then Martian counterparts are unlikely.

[50] Finally, the formation of valleys by groundwater weathering requires concomitant episodic high-intensity runoff from precipitation, either directly from rain or through snowmelt, in order to transport the products of seepage weathering from valley headwalls [*Howard and Kochel*, 1988; *Lamb et al.*, 2006]. In the most widely cited terrestrial example of valleys eroded into the Navajo Sandstone [e.g., *Laity and Malin*, 1985], it is unclear to what extent seepage weathering dominates valley extension as compared to erosion in plunge pools and headwall undermining at the contact between the Navajo Sandstone and the underlying Kayenta Formation [*Lamb et al.*, 2006].

[51] Although definitive identification of Martian fluvial networks as having been influenced by seepage processes may not be possible based upon remote sensing information, some valley networks exhibit morphologies that both resemble the simulated seepage-related valleys and which have a topographic context that might have encouraged groundwater involvement. One such setting is illustrated in Figure 8a, where a high plateau on the east side of the image lies about 1050 m above a northward-flowing drainage (Marikh Valles) that enters at the number sign and exits to the north at the at symbol. Several features of the tributary valleys dissecting the edges of this plateau suggest seepage-related erosion. Valleys eroded into the regional slope on the north side of the plateau exhibit flat-floored morphology and abrupt headwalls, e.g., the valleys in the top portion of Figure 8c and the valleys northeast of "z." Valleys eroded into the west side of the plateau exhibit a parallel drainage pattern with, again, abrupt terminations at a consistent elevation about 100 m below the plateau surface, as in Figures 8b and 8d and west of z. Both of these valley morphologies are typical of fluvial incision by seepage erosion or aided by seepage weathering (e.g., Figures 1e, 1f, and 5c). The broad, relatively undissected plateau surface could have served as a recharge area for seepage contributing to valley erosion. In Figure 8b a ledge near the head of the valleys suggests the outcrop of a resistant layer that could have encouraged seepage-related erosion by having served either as an aquifer or an aquiclude.

[52] However, surface runoff must also have occurred within the region shown in Figure 8. The crater at "x" has a deeply eroded valley extending from an exit breach on the southwest rim. The crater in Figure 8c also has an exit breach through the south rim. The plateau surface also is drained by a valley that has breached the divide at "y." These observations suggest that the valley networks may have had a composite origin involving both seepage-related erosion and surface runoff. The flat-floored valley heads in the top portion of Figure 8 may have received seepage discharge from standing water in the crater basin draining underground beneath the crater rim.

[53] In summary, the valley system dissecting the plateau in Figure 8 is consistent with joint involvement of surface runoff with either seepage weathering or seepage erosion. Alternatively, seepage processes might not have been important and the flat-floored valleys and parallel drainages may simply reflect fluvial erosion into a layered stratigraphy underlying the plateau.

6. Conclusions

[54] Our simulations have shown that erosion involving seepage processes produces a distinctive morphology of low-gradient flat-floored valleys with abrupt, theater-like headwalls and weak branching. Such valleys generally do not extend all the way to crater rims and major divides, and seepage-related valleys cutting into regional slopes commonly exhibit a parallel drainage pattern with headwalls at a consistent elevation on the regional slope. Seepage may be involved in valley incision either through direct erosion if the substrate is fine, cohesionless sediment or through aiding weathering of indurated sediment.

[55] Under the first scenario, the fine cohesionless sediments could be generated by impact cratering and weathering processes. However, groundwater seepage erosion could not form any integrated valley networks for sediment incorporating an appreciable fraction of gravel size or larger sediment. Seepage erosion tends to cause more incision at lower elevations. Erosion solely by runoff tends to cause more incision at higher elevations. In the second scenario, seepage weathering combined with fluvial runoff creates stubby deep canyons with abrupt headwalls that are similar in morphology to terrestrial and Martian valley systems attributed to erosion by groundwater. At least occasional

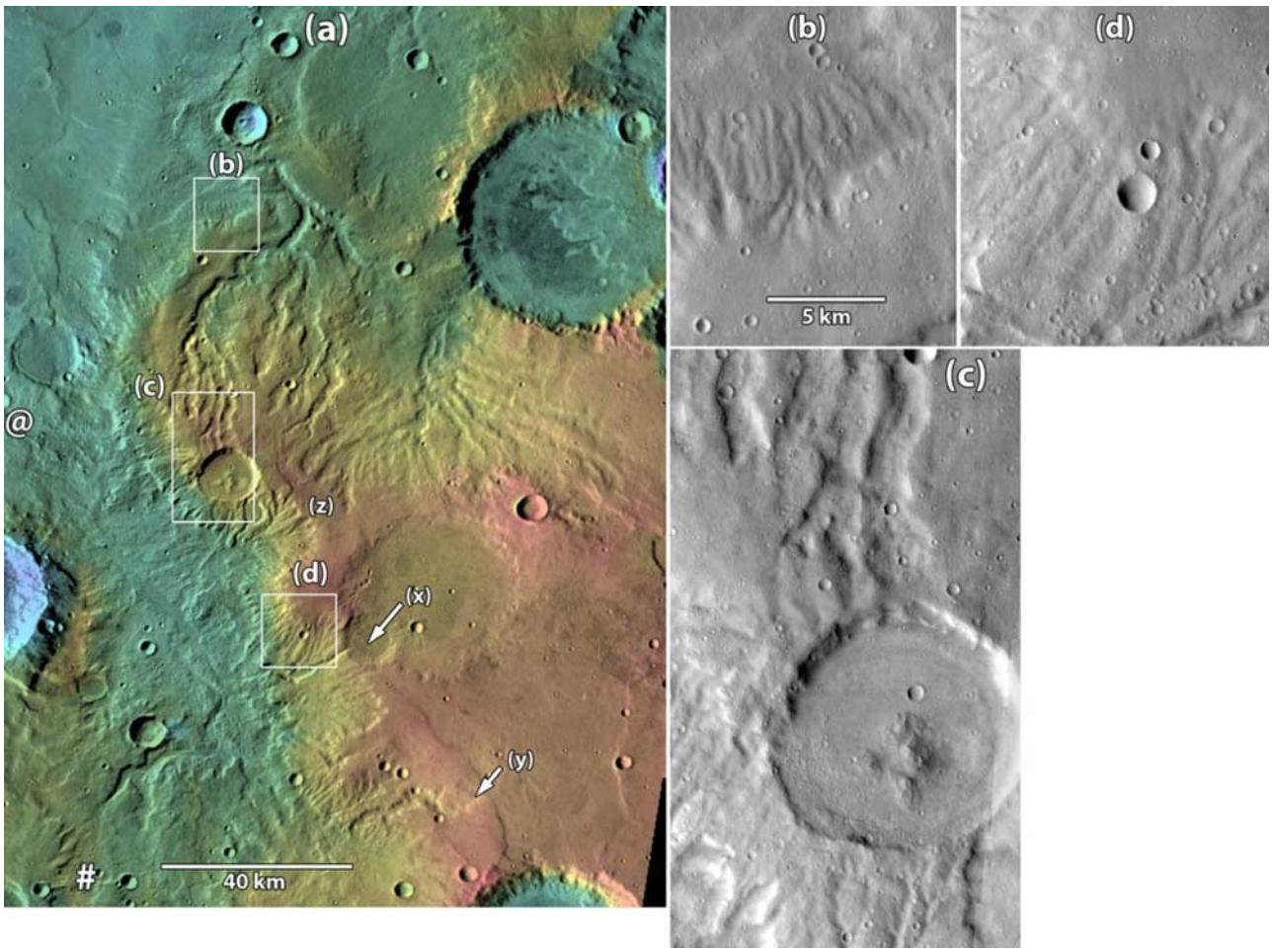

Figure 8. Martian plateau dissected by valleys possibly involving seepage-related erosion. (a) Thermal Emission Imaging System (THEMIS) daytime IR image mosaic with elevation color coding from Mars Orbiter Laser Altimeter PEDR topography. Image centered at about 5.8°E and 24.1°S. Boxes show location of insets. North is to top of image. (b) A portion of THEMIS visible light spectrometer (VIS) image V06317001. Scale applies to all insets. (c) A portion of VIS images V07428001 and V15615001. (d) A portion of VIS image V08152003. Images courtesy of Mars Space Flight Facility, Arizona State University at http://themis-data.asu.edu and Java Mission-Planning and Analysis for Remote Sensing at http://jmars.asu.edu/data.

direct runoff from precipitation is required to remove the weathering products of seepage weathering and mass-wasted debris produced by sapping of headwall cliffs. Thus we infer the role of groundwater in forming integrated Martian valley networks to be primarily through seepage weathering.

[56] Depending on seepage weathering rate, dissection of various degrees can be generated through seepage weathering. However, nonseepage related stratigraphic controls may produce valley morphology similar to that produced by seepage processes. In addition, postformation eolian modification may also make the landform resulted from sole surface runoff and that involving groundwater seepage similar both visually and from basin hypsometry, making interpretation difficult. Martian valley networks may have developed through a range of combinations of runoff erosion and seepage weathering, which can complicate the interpretation of the processes based on final landform morphology. Unequivocal identification of seepage involvement of valley incision on Mars may not be possible without knowledge of subsurface properties (hydraulic conductivity, layering, degree of cementation, etc.) and the grain sizes of sediment transported through the valley systems.

[57] **Acknowledgments.** This research is funded by NASA Mars Data Analysis Program. The authors would like to thank Vic Baker and Keith Harrison for their thorough and constructive reviews.

References

Brown, J. G., and J. H. Eychaner (1988), Simulation of five ground-water withdrawal projections for the Black Mesa area, Navaho and Hopi Indian Reservations, Arizona, *U. S. Geol. Surv. Water Resour. Invest. Rep.*, *88–4000*, 1–51.

Budhu, M., and R. Gobin (1995), Seepage-induced slope failures on sand-bars in Grand Canyon, *J. Geotech. Eng.*, *121*(8), 601–609, doi:10.1061/(ASCE)0733-9410(1995)121:8(601).

Carr, M. H. (1995), The Martain drainage system and the origin of valley networks and fretted channels, *J. Geophys. Res.*, *100*, 7479–7507, doi:10.1029/95JE00260.

Carr, M. H. (1996), *Water on Mars*, 229 pp., Oxford Univ. Press, New York.
Carr, M. H. (2002), Elevations of water-worn features on Mars: Implications for circulation of groundwater, *J. Geophys. Res.*, *107*(E12), 5131, doi:10.1029/2002JE001845.
Clifford, S., and T. Parker (2001), The evolution of the Martian hydrosphere: Implications for the fate of a primordial ocean and the current state of the Northern Plains, *Icarus*, *154*(1), 40–79, doi:10.1006/icar.2001.6671.
Clifford, S. M. (1993), A model for the hydrologic and climatic behavior of water on Mars, *J. Geophys. Res.*, *98*(E6), 10,973–11,016, doi:10.1029/93JE00225.
Coelho Netto, A. L., and N. F. Fernandes (1990), Hillslope erosion, sedimentation, and relief inversion in SE Brazil: Bananal, SP, in *Research Needs and Applications to Reduce Erosion and Sedimentation in Tropical Steeplands*, *Int. Assoc. Hydrol. Sci. Publ. Ser.*, vol. 192, edited by R. R. Ziemer et al., pp. 174–182, Int. Assoc. of Hydrol. Sci., Oxfordshire, U. K.
Craddock, R. A., and A. D. Howard (2002), The case for rainfall on a warm, wet early Mars, *J. Geophys. Res.*, *107*(E11), 5111, doi:10.1029/2001JE001505.
Dunne, T. (1980), Formation and controls of channel networks, *Prog. Phys. Geogr.*, *4*, 211–239, doi:10.1177/030913338000400204.
Dunne, T. (1990), Hydrology, mechanics, and geomorphic implications of erosion by subsurface flow, in *Groundwater Geomorphology: The Role of Subsurface Water in Earth-Surface Processes and Landforms*, edited by C. G. Higgins and D. R. Coates, pp. 1–28, *Geol. Soc. Am. Spec. Pap. Ser.*, vol. 252, Geol. Soc. of Am., Boulder, Colo.
Forsberg-Taylor, N. K., A. D. Howard, and R. A. Craddock (2004), Crater degradation in the Martian highlands: Morphometric analysis in the Sinus Sabaeus region and simulation modeling suggest fluvial processes, *J. Geophys. Res.*, *109*, E05002, doi:10.1029/2004JE002242.
Freeze, R. A., and J. A. Cherry (1979), *Groundwater*, 604 pp., Prentice-Hall, Englewood Cliffs, N. J.
Froede, C. R., Jr., and E. L. Williams (2004), The origin, development, and eventual consolidation of the canyons comprising Providence Canyon State Park, Stewart County, Georgia, *Southeast. Geol.*, *43*(1), 39–50.
Gabbard, D. S., C. Huang, L. D. Norton, and G. C. Steinhardt (1998), Landscape position, surface hydraulic gradients and erosion processes, *Earth Surf. Processes Landforms*, *23*(1), 83–92, doi:10.1002/(SICI)1096-9837(199801)23:1<83::AID-ESP825>3.0.CO;2-Q.
Gehrels, W. R., and O. Van De Plassche (1992), Origin of the paleovalley system underlying Hammock River marsh, Clinton, Connecticut, *J. Coastal Res.*, *11*, 73–83.
Gomez, B., and V. T. Mullen (1992), An experimental study of sapped drainage network development, *Earth Surf. Processes Landforms*, *17*, 465–476, doi:10.1002/esp.3290170506.
Grant, J. A. (2000), Valley formation in Margaritifer Sinus, Mars, by precipitation- recharged ground-water sapping, *Geology*, *28*(3), 223–226, doi:10.1130/0091-7613(2000)28<223:VFIMSM>2.0.CO;2.
Grant, J. A., and T. J. Parker (2002), Drainage evolution in the Margaritifer Sinus region, Mars, *J. Geophys. Res.*, *107*(E9), 5066, doi:10.1029/2001JE001678.
Gulick, V., and V. R. Baker (1989), Fluvial valleys and Martian palaeoclimates, *Nature*, *341*(6242), 514–516, doi:10.1038/341514a0.
Gulick, V. C. (1998), Magmatic intrusions and a hydrothermal origin for fluvial valleys on Mars, *J. Geophys. Res.*, *103*(E8), 19,365–19,387, doi:10.1029/98JE01321.
Gutierrez, B. T., E. Uchupi, N. W. Driscoll, and D. G. Aubrey (2003), Relative sea-level rise and the development of valley-fill and shallow-water sequences in Nantucket Sound, Massachusetts, *Mar. Geol.*, *193*(3–4), 295–314, doi:10.1016/S0025-3227(02)00665-5.
Hartmann, W. K., J. Anguita, M. A. de La Casa, D. C. Berman, and E. V. Ryan (2001), Martian cratering 7: The role of impact gardening, *Icarus*, *149*, 37–53, doi:10.1006/icar.2000.6532.
Heilweil, V. M., G. W. Freethey, C. D. Wilkowske, B. J. Stolp, and D. E. Wilberg (2000), Geohydrology and numerical simulation of ground-water flow in the central Virgin River basin of Iron and Washington Counties, Utah, *Tech. Publ. 116*, State of Utah Nat. Res., Salt Lake City.
Heilweil, V. M., T. S. McKinney, M. S. Zhdanov, and D. E. Watt (2007), Controls on the variability of net infiltration into desert sandstone, *Water Resour. Res.*, *43*, W07431, doi:10.1029/2006WR005113.
Higgins, C. G. (1982), Drainage systems developed by sapping on Earth and Mars, *Geology*, *10*(3), 147–152, doi:10.1130/0091-7613(1982)10<147:DSDBSO>2.0.CO;2.
Higgins, C. G. (1984), Piping and sapping: Development of landforms by groundwater outflow, in *Groundwater as a Geomorphic Agent*, edited by R. G. Lafleur, pp. 18–58, Allen and Unwin, St Leonards, N.S.W., Australia.
Howard, A. D. (1988), Groundwater sapping experiments and modeling, in *Sapping Features of the Colorado Plateau: A Comparative Planetary Geology Field Guide*, *NASA Spec. Publ. Ser.*, vol. 491, edited by A. D. Howard, R. C. Kochel, and H. E. Holt, pp. 71–83, NASA, Washington, D. C.
Howard, A. D. (1994), A detachment-limited model of drainage basin evolution, *Water Resour. Res.*, *30*(7), 2261–2286, doi:10.1029/94WR00757.
Howard, A. D. (1995), Simulation modeling and statistical classification of escarpment planforms, *Geomorphology*, *12*(3), 187–214, doi:10.1016/0169-555X(95)00004-O.
Howard, A. D. (1997), Badland morphology and evolution: Interpretation using a simulation model, *Earth Surf. Processes Landforms*, *22*(3), 211–227, doi:10.1002/(SICI)1096-9837(199703)22:3<211::AID-ESP749>3.0.CO;2-E.
Howard, A. D. (2007), Simulating the development of Martian highland landscapes through the interaction of impact cratering, fluvial erosion, and variable hydrologic forcing, *Geomorphology*, *91*, 332–363, doi:10.1016/j.geomorph.2007.04.017.
Howard, A. D., and R. C. Kochel (1988), Introduction to cuesta landforms and sapping processes on the Colorado Plateau, in *Sapping Features of the Colorado Plateau: A Comparative Planetary Geology Field Guide*, *NASA Spec. Publ.*, vol. 491, edited by A. D. Howard, R. C. Kochel, and H. E. Holt, pp. 6–56, NASA, Washington, D. C.
Howard, A. D., and C. F. McLane (1988), Erosion of cohesionless sediment by groundwater seepage, *Water Resour. Res.*, *24*(10), 1659–1674, doi:10.1029/WR024i010p01659.
Howard, A. D., and M. J. Selby (1994), Rockslopes, in *Geomorphology of Desert Environments*, edited by A. D. Abrahams and A. J. Parsons, pp. 123–172, Chapman and Hall, London.
Howard, A. D., J. M. Moore, and R. P. Irwin III (2005), An intense terminal epoch of widespread fluvial activity on Mars: 1. Valley network incision and associated deposits, *J. Geophys. Res.*, *110*, E12S14, doi:10.1029/2005JE002459.
Irwin, R. P., III, A. D. Howard, and R. C. Craddock (2006), Theater-headed valleys: The roles of overland flow and groundwater sapping, *Lunar Planet. Sci. [CD-ROM]*, *XXXVII*, abstract 1912.
Jones, J. A. A. (1971), Soil piping and stream channel initiation, *Water Resour. Res.*, *7*, 602–610, doi:10.1029/WR007i003p00602.
Jones, J. A. A. (1987), The effects of soil piping on contributing areas and erosion patterns, *Earth Surf. Processes Landforms*, *12*(3), 229–248, doi:10.1002/esp.3290120303.
Kochel, R. C., and J. F. Piper (1986), Morphology of large valleys on Hawaii: Evidence for groundwater sapping and comparison with Martian valleys, *J. Geophys. Res.*, *91*, E175–E192, doi:10.1029/JB091iB13p0E175.
Kochel, R. C., A. D. Howard, and C. McLane (1985), Channel networks developed by groundwater sapping in fine-grained sediments: Analogs to some Martian valleys, in *Models in Geomorphology*, edited by M. J. Woldenberg, pp. 313–341, Allen and Unwin, Winchester, Mass.
Kochel, R. C., D. W. Simmons, and J. F. Piper (1988), Groundwater sapping experiments in weakly consolidated layered sediments: A qualitative summary, in *Sapping Features of the Colorado Plateau: A Comparative Planetary Geology Field Guide*, *NASA Spec. Publ.*, vol. 491, edited by A. D. Howard, R. C. Kochel, and H. E. Holt, pp. 84–93, NASA, Washington, D. C.
Laity, J. E. (1983), Diagenetic controls on groundwater sapping and valley formation, Colorado Plateau, as revealed by optical and electron microscopy, *Phys. Geogr.*, *4*(2), 103–125.
Laity, J. E., and M. C. Malin (1985), Sapping processes and the development of theater-headed valley networks in the Colorado Plateau, *Geol. Soc. Am. Bull.*, *96*, 203–217, doi:10.1130/0016-7606(1985)96<203:SPATDO>2.0.CO;2.
Lamb, M. P., A. D. Howard, J. Johnson, K. X. Whipple, W. E. Dietrich, and J. T. Perron (2006), Can springs cut canyons into rock?, *J. Geophys. Res.*, *111*(E7), E07002, doi:10.1029/2005JE002663.
Lamb, M. P., A. D. Howard, W. E. Dietrich, and J. T. Perron (2007), Formation of amphitheater-headed valleys by waterfall erosion after large-scale slumping on Hawai'i, *Geol. Soc. Am. Bull.*, *119*(7–8), 805–822, doi:10.1130/B25986.1.
Lobkovsky, A. E., B. Jensen, A. Kudrolli, and D. H. Rothman (2004), Threshold phenomena in erosion driven by subsurface flow, *J. Geophys. Res.*, *109*, F04010, doi:10.1029/2004JF000172.
Luo, W. (2000), Quantifying groundwater sapping processes with a hypsometric analysis technique, *J. Geophys. Res.*, *105*(E1), 1685–1694, doi:10.1029/1999JE001096.
Luo, W., R. E. Arvidson, M. Sultan, R. Becker, M. K. Crombie, N. S. Sturchio, and Z. E. Alfy (1997), Ground-water sapping processes, Western Desert, Egypt, *Geol. Soc. Am. Bull.*, *109*(1), 43–62, doi:10.1130/0016-7606(1997)109<0043:GWSPWD>2.3.CO;2.
Malin, M. C., and M. H. Carr (1999), Groundwater formation of Martian Valleys, *Nature*, *397*, 589–591, doi:10.1038/17551.
Malin, M. C., and K. S. Edgett (2000), Evidence for recent groundwater seepage and surface runoff on Mars, *Science*, *288*, 2330–2335, doi:10.1126/science.288.5475.2330.

Mangold, N., and V. Ansan (2006), Detailed study of an hydrological system of valleys, a delta and lakes in the Southwest Thamasia region, Mars, *Icarus*, *180*(1), 75–87, doi:10.1016/j.icarus.2005.08.017.

Mangold, N., C. A. V. Quantin, and C. A. P. Delacourt (2004), Evidence for precipitation on Mars from dendritic valleys in the Valles Marineris area, *Science*, *305*(5680), 78–81, doi:10.1126/science.1097549.

Manning, C. E., and S. E. Ingebritsen (1999), Permeability of the continental crust: Implications of geothermal data and metamorphic systems, *Rev. Geophys.*, *37*(1), 127–150, doi:10.1029/1998RG900002.

Montgomery, D. R., and W. E. Dietrich (1989), Source areas, drainage density, and channel initiation, *Water Resour. Res.*, *25*(8), 1907–1918, doi:10.1029/WR025i008p01907.

Nash, D. J. (1996), Groundwater sapping and valley development in the Hackness Hills, North Yorkshire, England, *Earth Surf. Processes Landforms*, *21*(9), 781–795, doi:10.1002/(SICI)1096-9837(199609)21:9<781::AID-ESP616>3.0.CO;2-O.

Ni, W. J., and H. Capart (2006), Groundwater drainage and recharge by networks of irregular channels, *J. Geophys. Res.*, *111*, F02014, doi:10.1029/2005JF000410.

Nwankwor, G. I., C. E. Dike, and C. J. Iwuagwu (1998), Piping, quick conditions and liquefaction as factors of gully erosion: A case study of Okwudor-Amucha gully complex, Imo State, Nigeria, *J. Min. Geol.*, *34*(2), 225–230.

Onda, Y. (2002), The effect of soil piping at seepage face on slope stability and landform development, *Trans. Jpn. Geomorphol. Union*, *23*(4), 647–658.

Otvos, E. G. (1999), Rain-induced beach processes; landforms of ground water sapping and surface runoff, *J. Coastal Res.*, *15*(4), 1040–1054.

Pieri, D. C. (1980a), Geomorphology of Martian valleys, in *Advances in Planetary Geology*, *NASA Tech. Memo. 81979*, 1–362, NASA, Washington, D. C.

Pieri, D. C. (1980b), Martian valleys: Morphology, distribution, age, and origin, *Science*, *210*, 895–897, doi:10.1126/science.210.4472.895.

Saar, M. O., and M. Manga (2004), Depth dependence of permeability in the Oregon Cascades inferred from hydrogeologic, thermal, seismic, and magmatic modeling constraints, *J. Geophys. Res.*, *109*, B04204, doi:10.1029/2003JB002855.

Schumm, S. A. (1977), *The Fluvial System*, John Wiley, New York.

Schumm, S. A., and L. Phillips (1986), Composite channels of the Canterbury Plain, New Zealand: A Martian analog?, *Geology*, *14*(4), 326–329, doi:10.1130/0091-7613(1986)14<326:CCOTCP>2.0.CO;2.

Schumm, S. A., K. F. Boyd, C. G. Wolff, and W. J. Spitz (1995), A groundwater sapping landscape in the Florida panhandle, *Geomorphology*, *12*(4), 281–297, doi:10.1016/0169-555X(95)00011-S.

Sharp, R. P., and M. C. Malin (1975), Channels on Mars, *Geol. Soc. Am. Bull.*, *86*(5), 593–609, doi:10.1130/0016-7606(1975)86<593:COM>2.0.CO;2.

Shorghofer, N., B. Jensen, A. Kudrolli, and D. H. Rothman (2004), Spontaneous channelization in permeable ground: Theory, experiment, and observation, *J. Fluid Mech.*, *503*, 357–374, doi:10.1017/S0022112004007931.

Spence, C. D., and D. J. Sauchyn (1999), Groundwater influence on valley-head geomorphology, upper Battle Creek basin, Alberta and Saskatchewan, *Bull. Geol. Surv. Can.*, *534*, 249–255.

Teixeira De Oliveira, M. A. (1990), Slope geometry and gully erosion development: Bananal, Sao Paulo, Brazil, *Z. Geomorphol.*, *34*(4), 423–434.

Thomas, B. E. (2002), Ground-water, surface-water, and water-chemistry data, Black Mesa Area, northeastern Arizona–200–2001, and performance and sensitivity of the 1988 USGS numerical model of the N aquifer, *U. S. Geol. Surv. Water Resour. Invest. Rep.*, *2002–4211*, 1–75.

Tomlinson, S. S., and Y. P. Vaid (2000), Seepage forces and confining pressure effects on piping erosion, *Can. Geotech. J.*, *37*(1), 1–13, doi:10.1139/cgj-37-1-1.

Uchupi, E., and R. N. Oldale (1994), Spring sapping origin of the enigmatic relict valleys of Cape Cod and Martha's Vineyard and Nantucket Islands, Massachusetts, *Geomorphology*, *9*(2), 83–95, doi:10.1016/0169-555X(94)90068-X.

Zhu, C. (2000), Estimate of recharge from radiocarbon dating of groundwater and numerical flow and transport modeling, *Water Resour. Res.*, *36*(9), 2607–2620, doi:10.1029/2000WR900172.

A. D. Howard, Department of Environmental Sciences, University of Virginia, 291 McCormick Road, Charlottesville, VA 22903, USA. (ah6p@virginia.edu)

W. Luo, Department of Geography, Northern Illinois University, Davis Hall, Room 118, DeKalb, IL 60115, USA. (wluo@niu.edu)